Analysis of Bore Characteristics Using KdV-Based Nonlinear Fourier Transform

Brühl, M.; Wahls, S.; Barranco Granged, Ignacio; Liu, Philipp L.-F.

DOI
10.1115/OMAE2020-19074

Publication date
2020

Document Version
Accepted author manuscript

Published in
Proceedings of the ASME 2020 39th International Conference on Ocean, Offshore and Arctic Engineering, OMAE 2020

Citation (APA)
Brühl, M., Wahls, S., Barranco Granged, I., & Liu, P. L.-F. (2020). Analysis of Bore Characteristics Using KdV-Based Nonlinear Fourier Transform. In *Proceedings of the ASME 2020 39th International Conference on Ocean, Offshore and Arctic Engineering, OMAE 2020* (Vol. Volume 6B: Ocean Engineering). Article OMAE2020-19074 ASME. https://doi.org/10.1115/OMAE2020-19074

Proceedings of the ASME 2020 39th International & Conference on Ocean, Offshore and Arctic Engineering
OMAE2020
June 28-July 3, 2020, Fort Lauderdale, FL, USA

OMAE2020-19074

ANALYSIS OF BORE CHARACTERISTICS USING KDV-BASED NONLINEAR FOURIER TRANSFORM

Markus Bruehl*, Sander Wahls
Delft Center of Systems and Control (DCSC)
Delft University of Technology
Delft, 2628 CD
The Netherlands
Email: m.bruehl@tudelft.nl

Ignacio Barranco Granged, Philipp L.-F. Liu
Department of Civil and Environmental Engineering
National University of Singapore (NUS)
Singapore

ABSTRACT

Bores propagating in shallow water transform into undular bores and, finally, into trains of solitons. The observed number and height of these undulations, and later discrete solitons, is strongly dependent on the propagation length of the bore. Empirical results show that the final height of the leading soliton in the far-field is twice the initial mean bore height. The complete disintegration of the initial bore into a train of solitons requires very long propagation lengths, but unfortunately these required distances are usually not available in experimental tests or nature. Therefore, the analysis of the bore decomposition for experimental data into solitons is difficult and requires further approaches. Previous studies have shown that by application of the nonlinear Fourier transform based on the Korteweg–de Vries equation (KdV-NFT) to bores and long-period waves propagating in constant depth, the number and height of all solitons can be reliably predicted already based on the initial bore-shaped free surface.

Against this background, this study presents the systematic analysis of the leading-soliton amplitudes for non-breaking and breaking bores with different strengths in different water depths in order to validate the KdV-NFT results for non-breaking bores, and to show the limitations of wave breaking on the spectral results. The analytical results are compared with data from experimental tests, numerical simulations and other approaches from literature.

INTRODUCTION

In coastal, shallow regions, tsunamis or other long-period waves often propagate as bore-shaped waves that will first evolve into undular bores and later, in case of sufficient long propagation length, into trains of solitons. In both cases, the first undulation or the leading solitons will show significant amplification compared to the initial bore height. Knowledge about these processes will help to understand the underlying processes and to predict the bore evolution from near- to far-field.

Experimental tests and numerical simulations confirm that, in case of sufficient propagation length, significant transformations within undular bores lead to discrete solitons emerging out the bore front. For bores propagating on a horizontal bed, the far-field leading-soliton amplitudes A_1 reach up to twice the initial bore height η_b [1, 2, 3]. Furthermore, as function of the bore length a number of rank-ordered solitons can arise from the bore. Thus, the processes of undular bore generation and amplification of the maximum crest elevation as the solitons emerge out of the bore front provide a significant thread to downwave locations.

With the nonlinear Fourier transform based on the Korteweg–de Vries equation (KdV-NFT), a powerful analysis technique is available that uses nonlinear cnoidal waves as the spectral basis for the decomposition of the original data. [4,5,6,7] The application of this method to experimental and numerical bore data allows to identify the underlying solitons that are already present in the initial bore shape, although they cannot be seen directly due to the superposition with their strong nonlinear

*Address all correspondence to this author.

wave-wave interactions. [8] Within the nonlinear decomposition in KdV-NFT, the spectral so-called cnoidal basic components (solitons and oscillatory waves) are identified and separated from their nonlinear interactions. Finally, the spectral results are presented in the so-called nonlinear spectrum in a similar way to the conventional linear Fourier spectrum. [4]

By comparison of nonlinear spectra obtained from experimental gauge data at different positions along the bore propagation and numerical simulations of the tempo-spatial evolution of these bores, it has been shown that the nonlinear spectra for a propagating undular, non-breaking bore is nearly constant [8]. This result is remarkable because although the free surface changes significantly from a trapezoidal-shaped initial bore into an undulating bore and, finally, into a train of discrete solitons, the underlying nonlinear spectral components are the same for all timesteps and positions. Thus, the variation of the free surface is solely caused by the strength and shape of the nonlinear wave-wave interactions between these invariant spectral components. Finally, this implies that for non-breaking bores in constant depth the KdV-NFT analysis of the initial bore will provide all required information for the understanding and prediction of the downwave bore propagation, including the number and peaks of the undulations within the bore as well as the number and amplitudes of the far-field solitons.

In this paper, leading-soliton amplitudes for non-breaking and breaking bores with different strengths in different water depths are analysed systematically in order to validate the KdV-NFT results for non-breaking bores, and to show the limitations of wave breaking on the spectral results. The analytical results are compared with data from experimental tests, numerical simulations and other approaches from literature.

THEORETICAL BACKGROUND

Properties of paddle-generated bores in the wave flume

The properties of non-breaking undular bores can be derived from the mass and momentum conservation equations that provide the nonlinear shallow water equation. This approach presumes the horizontal flow velocities $u(x,y,t)$ to be unitary over depth h so that $\partial u/\partial y = u_y = 0$ and thus $u = u(x,t)$, the pressure distribution over depth $p(h)$ to be hydrostatic, and the liquid to be inviscid. Then, the mass conservation relation derived in [9] defines the relation between bore height, celerity and depth as

$$h_b\,(U_b - u_b) = h_0\,(U_b - u_0)\,, \tag{1}$$

with depth under the bore h_b from Eq. (2) and fluid velocity behind the bore u_b, that propagate with bore celerity U_b into water with initial depth h_0 and initial fluid velocity u_0, with $u_b > u_0 \geq 0$ as defined in Fig. 1a,b.

The relation between the bore height h_b over the bottom and the bore height η_b over the still water level (SWL) is

$$h_b = (\eta_b + h_0). \tag{2}$$

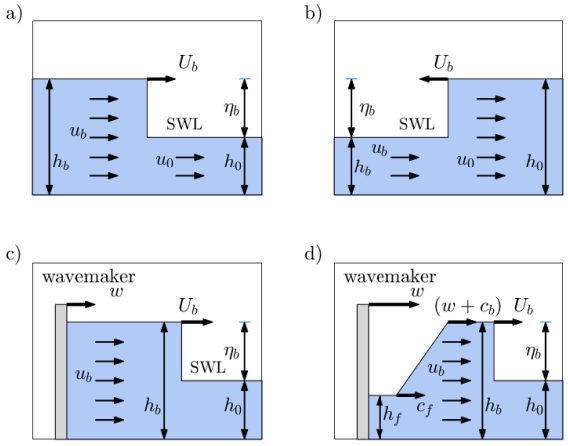

FIGURE 1: DEFINITION OF KEY PARAMETERS FOR a) A BORE PROPAGATING DOWNSTREAM THE FLUME, b) A HYDRAULIC JUMP UPSTREAM THE FLUME, c) BORE ACCUMULATION DURING CONSTANT VELOCITY OF THE PADDLE, AND d) THE PROPAGATION OF THE BORE AFTER THE PADDLE HAS STOPPED (AFTER [9]).

Within this study, the propagation of the free surface is characterized by the strength of the bore in terms of the dimensionless bore Froude number [10, 11]

$$\mathrm{Fr}_b = \frac{U_b - u_0}{\sqrt{g h_0}}, \tag{3}$$

with g the acceleration due to gravity, U_b the bore-front celerity, and u_0 the initial fluid velocity at initial depth h_0.

Consideration of the relations between water depth h_0 and bore celerity U_b in both directions of the bore provides the function for the strength of the bore [12]

$$\frac{h_b}{h_0} = \left(\frac{c_b}{c_0}\right)^2 = \frac{1}{2}\left(\sqrt{1+8\mathrm{Fr}_b^2} - 1\right), \tag{4}$$

where $c_0 = \sqrt{g h_0}$ and $c_b = \sqrt{g h_b}$ are the wave celerities in the initial depth h_0 in front of and in depth h_b behind the bore front. Further details on the bore properties and the relation between paddle motion and bore height can be found in [8].

Based on the bore Froude number Fr_b, bores show different characteristics of wave propagation. According to literature, three different types of bore waves in function of their strength can be defined: i) *Undulating bores* show values $\mathrm{Fr}_b \leq 1.25$ [13]. ii) *Fully developed bores* are described by [10] for values $\mathrm{Fr}_b \geq 1.55$. iii) *Breaking bores* are obtained when bores with $\mathrm{Fr}_b > 1.25$ start to break. However, other values can also

be found in the literature. Therefore, the limit between breaking and non-breaking undular bores is located in the range between $1.2 \leq \mathrm{Fr}_b \leq 1.53$ and for breaking and fully developed bores between $1.42 \leq \mathrm{Fr}_b \leq 1.8$ [10, 11, 14, 15, 16]. The focuses of recent analytical and numerical studies show that clear definitions of limits for the bore regimes and the evolution of undular bores require further research [17].

Within this study, experimental data from non-breaking and breaking undular bores are analysed in order to validate the ability of the KdV-NFT to determine the far-field solitons from near-field data. As can be seen in Tab. 1, the nominal bore Froude numbers for these tests are in the range of $1.10 \leq \mathrm{Fr}_b \leq 1.50$ which is in accordance with the values obtained from literature for non-breaking bores.

Solitons and their connection to undular bores

A soliton (or solitary wave) is a translatory wave of permanent shape with only one crest and no troughs. In constant depth, solitons can propagate over long distances without changes in shape. Furthermore, when interacting with other solitons or nonlinear waves they preserve their shape and re-appear from the interaction process with identical shape and celerity, but a shift in phase. The analytical form of the soliton for the lowest-order KdV equation for a single positive wave pulse and its amplitude-dependent phase speed are given as [18]:

$$\eta(x,t) = \eta_0 \operatorname{sech}^2\left(\sqrt{\frac{3}{4}\frac{\eta_0}{h_0^3}}\,(x - ct - \varphi_0)\right), \tag{5}$$

$$c = c_0\left(1 + \frac{\eta_0}{2h_0}\right), \tag{6}$$

where $\eta(x,t)$ is the free-surface displacement, η_0 the soliton amplitude (note that for solitary waves that have no wave trough the wave amplitude η_0 is identical with the wave height H, thus $\eta_0 = H$), x and t the variables for position and time, φ_0 the initial position of the soliton crest at $t = 0$, h_0 the initial water depth in which the soliton is propagating , c the nonlinear phase speed of the soliton, and $c_0 = \sqrt{gh_0}$ the wave celerity in shallow water.

As can be seen in Eq. (6), the nonlinear phase speed or celerity c of the soliton is a function of the wave height η_0. Thus, the larger the soliton the faster it propagates, up to the point of wave breaking according to the breaking criterion[1] [20]. At this maximum height A_{max}, the mathematical formulation in Eq. (5) starts to be become unphysical:

$$\frac{A_{max}}{h_0} = 0.83. \tag{7}$$

The mathematical representation of the soliton in Eq. (5) is an exact solution of the nonlinear Korteweg–de Vries (KdV) equation in Eqs. (14) and (17), that describes the propagation of long-period waves in shallow water. For solitons, the nonlinear and the dispersive terms in the KdV equation are exactly counterbalanced. Therefore, the wave does neither break or disperse but preserves its shape over long propagation distances while propagating in constant depth. Furthermore, even after interaction processes such as overtaking of solitons or other nonlinear wave-wave interactions they regain their old shapes once the interactions have ceased. Thus, if an initial bore-shaped free-surface near field signal consists of (hidden) solitons, then in the far-field and after a particular time and distance, these solitons emerge from of the undulating non-breaking bore and form trains of solitons with different amplitudes in the far field. Due to the amplitude dispersion of the solitons, their celerity is increasing with their height, and the larger solitons propagate faster within the bore. With increasing distance between the soliton positions, the nonlinear interactions suppressing the real solitons shape decrease. Finally, the larger solitons leave the bore behind earlier than the lower ones and become visible as discrete rank-ordered solitons without significant interactions. [8]

If the initial bore height η_b is known, e.g. as the mean bore plateau height $\overline{\eta_b}$ before the undulations start (as used within this study), then the final soliton amplitude A_1 of the leading, largest soliton can be expected to be [1, 2, 3]

$$A_1 = 2\eta_b = 2(h_b - h_0), \tag{8}$$

where A_1 is the amplitude of the first, leading soliton in the far-field, $\eta_b = \overline{\eta_b}$ the (mean) height of the bore above SWL, h_b from Eq. (2) the depth behind the bore front, and h_0 the depth in front of the bore (see Fig. 1).

Theoretical bore parameters

Based on the equations given above, for given Froude numbers Fr_b some parameters of the propagating bores can be calculated such as the expected bore height η_b, the expected height A_1 of the leading soliton, the relative bore height $(h_b/h_0)_{b,\mathrm{br}}$ and the bore Froude number $\mathrm{Fr}_{b,\mathrm{br}}$ for the breaking limit. These parameters will be used later for the validation of the experimental data and the results obtained from KdV-NFT.

Application of the breaking criterion in Eq. (7) provides the maximum relative soliton amplitude A_{max} before breaking. Combination with Eq. (8) gives

$$A_{max} = 0.83h_0 = 2\eta_{b,\mathrm{br}}, \tag{9}$$

$$\eta_{b,\mathrm{br}} = 0.415h_0, \tag{10}$$

with $\eta_{b,\mathrm{br}}$ the maximum bore height for non-breaking solitons. For the relative bore height h_b/h_0 in the breaking limit applies

$$(h_b/h_0)_{b,\mathrm{br}} = 1.415. \tag{11}$$

The calculated amplitude of the leading solitons can be obtained

[1] The analysis of landslide-induced waves in [19] show that the breaking criterion of $\eta_0 = 0.83h_0$ by Lenau [20] fits better with the KdV-NFT results than the older, but more common criterion of $\eta_0 = 0.78h_0$ by McCowan [21].

from Eqs. (2), (8) and (11):

$$A_1(h_b/h_0) = 2\left[\left(\frac{h_b}{h_0}\right)h_0 - h_0\right]. \tag{12}$$

Resolving Eq. (4) for Fr_b and consideration of Eq. (2) yields the bore Froude number $\mathrm{Fr}_{b,\mathrm{br}}$ for the maximum non-breaking soliton amplitude:

$$\mathrm{Fr}_{b,\mathrm{br}} = \sqrt{\frac{\left(\frac{2h_b}{h_0}+1\right)^2-1}{8}} = \sqrt{\frac{\left(\frac{2.83h_0}{h_0}+1\right)^2-1}{8}} = 1.307. \tag{13}$$

Nonlinear Fourier transform based on the Korteweg–de Vries equation

The KdV equation was proposed by Korteweg and de Vries [22] to describe the evolution of the free surface $\eta(x,t)$ of long, unidirectional surface waves in shallow-water ($h/L < 0.22$) in space and time (with h the depth and L the wavelength). For the analysis of space series $\eta(x,0)$ (initial value problem), the space-like KdV (sKdV) equation is applied. The dimensional form of the sKdV is given as [7, 23, 24]:

$$\eta_t + c\eta_x + \alpha\eta\eta_x + \beta\eta_{xxx} = 0, \quad 0 \le x \le L_w, \tag{14}$$

with $\eta(x,t)$ the free surface elevation as a function of space x and time t, the subscripts related to the partial derivatives of $\eta(x,t)$ with respect to x and t, $\eta_t = \partial\eta/\partial t$ the vertical velocity of $\eta(x,t)$, $\eta_x = \partial\eta/\partial x$ the partial derivative in wave direction x, η_{xxx} the third-order partial derivative in space x, $\alpha\eta\eta_x$ the nonlinear convective term, $\beta\eta_{xxx}$ the dispersive term, and L_w the length of the analysis window in space domain. The wave celerity or linear phase speed in shallow-water c, the coefficients α for nonlinearity, β for dispersion and the relation λ between nonlinearity and dispersion strongly depend on the particular physical application and the boundary conditions, especially on water depth h. For progressive surface waves in space domain applies [7]

$$c = \sqrt{gh}, \quad \alpha = \frac{3c}{2h}, \quad \beta = \frac{ch^2}{6}, \quad \lambda = \frac{\alpha}{6\beta} = \frac{3}{2h^3}, \tag{15}$$

where g is the acceleration due to gravity. Eq. (14) has the linear dispersion relation

$$\omega = ck - \beta k^3, \tag{16}$$

where k and ω are the wave number $k = 2\pi/L$ and the angular frequency $\omega = 2\pi/T$, with L the wave length and T the wave period.

For the analysis of time series and the boundary value problem $\eta(0,t)$ the time-like KdV equation (tKdV) is applied, which is derived from the sKdV equation by changing the space and time variables: $x \to t$ and $t \to x$, $k \to \omega$ and $\omega \to k$ [25]:

$$\eta_x + c'\eta_t + \alpha'\eta\eta_x + \beta'\eta_{xxx} = 0, \quad 0 \le x \le T_w, \tag{17}$$

with the modified time-domain coefficients from Eq. (15)

$$c' = \frac{1}{c} = \frac{1}{\sqrt{gh}}, \quad \alpha' = -\frac{\alpha}{c^2}, \quad \beta' = -\frac{\beta}{c^4}, \quad \lambda' = \frac{\alpha'}{6\beta'} = \frac{3c^2}{2h^3}, \tag{18}$$

and T_w the length of the analysis window in time domain. Since the experimental gauge data are available as time series, the tKdV is applied for the further analyses within this study.

Solitary-wave solutions as discussed in [26, 27] provide translatory solitons as solutions for the KdV equation. By application of a mathematical procedure called inverse scattering transform (IST) [28], the KdV equation can be solved also for periodic travelling-wave boundary conditions in terms of so-called cnoidal waves [22]. Due to the analogy of this method compared to the application of conventional fast Fourier transform (FFT), the solution of the KdV equation by application of the IST is called KdV-based nonlinear Fourier transform (KdV-NFT), even if this approach is much more complex than the FFT. In engineering terminology the IST of the KdV equation might be considered as an extension or – even better – as a substitute of the conventional linear FT by a generalized NFT for shallow-water waves. Nevertheless, for initial conditions that evolve strictly linearly, the NFT provides the same results as conventional FFT.

The main feature of periodic NFT is that the initial signal is decomposed into nonlinear cnoidal waves that are physical representations of nonlinear shallow-water waves instead of linear sinusoidal spectral basic components as in FFT. Therefore, this method is perfect for the spectral decomposition of coastal wave data into realistic shallow-water waves (the cnoidal waves) and their nonlinear interactions. Since the KdV-NFT is based on the KdV equation, it is strictly valid only for $kh \le 1.0$, which describes the range of validity of the KdV equation. With regard to the nonlinear interactions, for practical applications this value can be extended to $kh < 1.36$ ($h/L < 0.22$) [7]. For values $kh \ge 1.36$, the nonlinear wave-wave interactions are governed by the nonlinear Schroedinger equation and no longer by KdV equation [7].

The most important and fascinating feature of the KdV-NFT approach is its ability to decompose given experimental or numerical shallow-water surface-wave data in time domain, $\eta(x_0, t)$, or space domain, $\eta(x, t_0)$, explicitly into N constitutive nonlinear cnoidal-wave time-domain components $\eta_{\mathrm{cn},i}$ and the sum of their nonlinear wave-wave interaction terms $\sum_j \eta_{\mathrm{int},j}$ [29]. For the analysis of time-domain data applies:

$$\underbrace{\eta(x_0,t)}_{\text{given data}} = \underbrace{\sum_i^N \eta_{\mathrm{cn},i}(x_0,t)}_{\text{sum of cnoidal waves}} + \underbrace{\sum_j \eta_{\mathrm{int},j}(x_0,t)}_{\text{nonlinear interactions}}. \tag{19}$$

The decomposition of the initial data into cnoidal waves and interactions is called the direct KdV-NFT (dKdV-NFT). The nonlinear superposition of these cnoidal waves in the inverse nonlinear Fourier Transform (iKdV-NFT), including the calcu-

lation and summation of the nonlinear interactions according to Eq. (19), returns the given data $\eta(x_0,t)$. The interaction terms $\eta_{\mathrm{int},j}(x_0,t)$ in Eq. (19) are not provided by the dKdV-NFT, but are calculated within the iKdV-NFT (see [30]).

Due to the nonlinear interactions, the underlying spectral structure of this set of cnoidal-wave basic components cannot be obtained directly from the free surface elevation $\eta(x_0,t)$ (except for $N=1$). The KdV-NFT is realized by solving a Schroedinger eigenvalue problem. Therefore, the so-called Floquet discriminant $\Delta(E)$ of the original data is obtained as the trace of the so-called monodromy matrix. For details see [7,4]. The spectral results are strongly depend on the characteristics of the analysed data $\eta(x_0,t)$ and especially the water depth (see [5]). For an undular bore, the nonlinear spectra obtained from KdV-NFT remain constant as the bore propagates in constant depth and changes its shape from trapezoidal shape over undular bores up to a trains of solitons. [8]. On the other hand, if the same input data are analysed for different water depths then the nonlinear spectra change in function of depth [31].

From the Floquet discriminant $\Delta(E)$ the number N of the determined cnoidal waves, their moduli m_i, amplitudes a_i, wave numbers k_i or frequencies ω_i or f_i, and phases φ_i are determined. Based on the determined values of m_i, the cnoidal waves can be classified as oscillatory waves (for $m_i \leq 0.99$) with the parameters a_i, k_i, ω_i or f_i and φ_i, or solitons (for $m_i > 0.99$) with A_j, K_j, Ω_i or F_j and Φ_j. In order to better distinguish between oscillatory waves and solitary waves (solitons), the parameters of the solitary waves are denoted by capital letters.

For the illustration of the nonlinear spectrum obtained from KdV-NFT, Fig. 2 shows the spectral results for the undular bore from numerical simulation as given in the upper-right corner of the figure. The representation is very similar to the conventional FFT spectrum. The nonlinear spectrum consists of the radiation spectrum (right part) with the spectral parameters of the oscillatory ('radiation') waves (amplitudes a as blue line), and the soliton spectrum (left part) with the soliton amplitudes A (red bars). The so-called 'reference level' separates both parts of the spectrum. Furthermore, for each component the modulus m is given (dashed line). In order to clearly distinguish between oscillatory and solitary waves in the spectrum, the latter are plotted with frequencies smaller than those of the oscillatory waves, including negative frequencies F or wave numbers K. Within the analysis, wave numbers and frequencies for solitons are determined as complex numbers. The values for F and K as given in the plot are the absolute values of the imaginary part with reverse signs. Naturally, $F=1$ and $K=1$ applies for all solitons in the spectrum, but they values used here sort the amplitudes within the spectrum according to their height and avoids the overlay of all solitons at one position on the right axis or the introduction of the complex plane. The degree of nonlinearity of each cnoidal basic component $\eta_{\mathrm{cn},i}(x,t)$ is defined by its modulus m_i. For a given water depth the nonlinearity, and thus the modulus m_i, generally

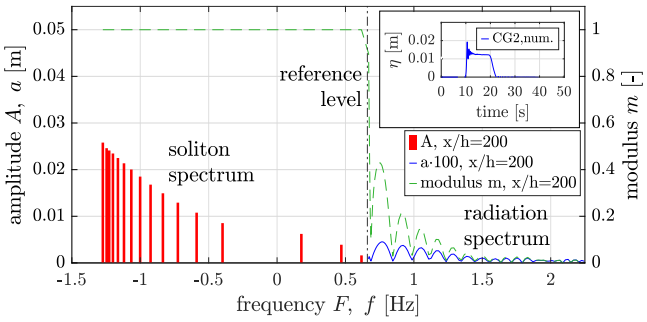

FIGURE 2: KdV-NFT SPECTRUM OF THE TIME SERIES OBTAINED AT GAUGE CG2'.

decreases with increasing k_i or f_i for each oscillatory component i, because the latter implies that the relative water depth h/L_i increases. Further details on the mathematical and numerical background of the methods are given in [7,5,4].

EXPERIMENTAL SET-UP, TEST PROGRAMME, AND NUMERICAL SIMULATIONS

Experimental set-up

Experimental tests with bores with different strengths and different water depths were conducted in the wave flume in the Hydraulic Engineering Laboratory at National University of Singapore (NUS) (see Fig. 3). The wave flume has a length of 36 m, and both width and height are 0.9 m. The flume is equipped with a novel piston-type wave maker with a stroke $s_{max} = 5\,\mathrm{m}$, velocity $v_{max} = 2\,\mathrm{m/s}$, and acceleration $a_{max} = 3.5\,\mathrm{m/s^2}$ that allows the generation of long-period waves and bores.

The bores are generated by accelerating the piston-type paddle from the initial position x_i and velocity $w_i = 0$ with constant acceleration $a = const.$ to the desired paddle velocity w, then moving the paddle with this constant velocity w, and finally decelerating the paddle with deceleration $d = -a$ (unless another value for d is selected) back to the final paddle velocity $w_f = 0$. Thus, a trapezoidal shape of the initial free surface is obtained. The generated surface displacement of the propagating bore is measured with four capacity gauges CG1 to CG4 at positions $x = 5.193$ m, 9.887 m, 14.882 m, and 18.869 m (see Fig. 3), with CG1 being located 0.193 m behind the maximum-stroke position of the wave paddle. The positions of the wave gauges were selected in combination with the test programme so that at all four gauges the complete bore is captured, including ramping-up at the bore front and ramping-down at the bore back.

Test programme

For the bore tests considered within this study, different nominal values for water depth h_0, paddle stroke s, and paddle

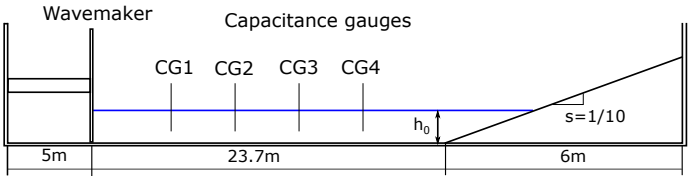

FIGURE 3: EXPERIMENTAL SET-UP IN THE WAVE FLUME AT NUS.

TABLE 1: LIST OF NOMINAL VALUES FOR BORE FROUDE NUMBER $\mathrm{Fr}_{b,\mathrm{nom}}$, DEPTH h_0, PADDLE STROKE, ACCELERATION, DECELERATION AND VELOCITY, s, a, d, AND v.

parameter	nominal values
$\mathrm{Fr}_{b,\mathrm{nom}}$ [−]	1.10, 1.15, 1.20, 1.25, 1.275, 1.30, 1.35, 1.40, 1.45, 1.50
h_0 [m]	0.10, 0.20
s [m]	2.00, 2.50, 3.00, 4.00, 4.50, 5.00
a [m/s^2]	0.100
d [m/s^2]	-0.100, -3.500
v_{nom} [m/s]	0.127, 0.181, 0.188, 0.249, 0.268, 0.308, 0.338, 0.354, 0.367, 0.425, 0.439, 0.481, 0.488, 0.545, 0.602

velocity v_{nom} have been set as input parameters for the wave generation. The total variation of the selected input values is listed in Tab. 1. The values have been obtained based on the nominal bore Froude numbers $\mathrm{Fr}_{b,\mathrm{nom}}$ as given in the table. For the analyses and Fig. 7, the values for Fr_b as obtained from the experimental test data are used. The paddle acceleration and deceleration were set to $a = 0.100\,\mathrm{m/s}$ and $d = -0.100\,\mathrm{m/s}$ (except one test with $d = -3.500\,\mathrm{m/s}$).

Numerical simulations

The results of the experimental tests show that the available flume length allows the formation of undular bores, but the complete disintegration of the initial bore into solitons cannot be observed. Therefore, we conducted numerical simulations with the model COULWAVE [32] in order to obtain the far-field soliton trains. The data measured in the experimental tests at gauge CG1 ($x = 5.193\,\mathrm{m}$) are used as input for the simulations. The results at numerical gauges at $x = 0.01$ m and at numerical positions CG2', CG3' and CG4' ($x' = 4.694\,\mathrm{m}$, $9.689\,\mathrm{m}$ and $13.676\,\mathrm{m}$) according

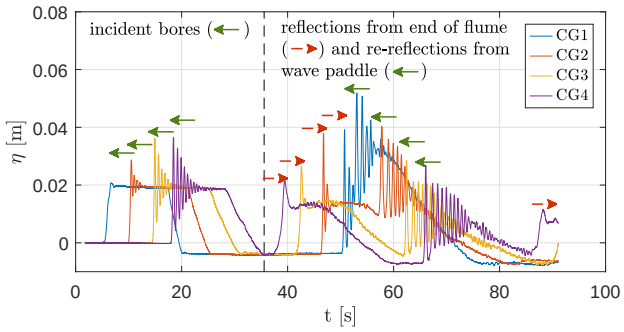

FIGURE 4: EXAMPLE FOR EXPERIMENTAL BORE DATA, MEASURED AT GAUGES CG1 TO CG4. ONLY THE INCIDENT BORES ARE CONSIDERED FOR FURTHER ANALYSIS.

to the experimental gauges are used to compare the near-field data and to verify the quality of the numerical results. The example in Fig. 5 shows the numerical simulation with the initial trapezoidal-shaped bore at CG1 (blue line in Fig. 4) as input signal. The trough behind the initial bore and the reflections are neglected and replaced by zeros in the simulation input data. The plots in Fig. 5 compare the experimental data at gauges CG2 to CG4 (blue lines) with the numerical results at numerical gauges CG2' to CG4' at the according positions x' (red lines). The results show good agreements between the experimental and the numerical results for the propagating bore. Therefore, COULWAVE is regarded to correctly simulate the bore propagation, and the far-field simulation data are assumed to be reliable.

The far-field data at positions $x' = 100\,\mathrm{m}$, $200\,\mathrm{m}$ and $230\,\mathrm{m}$ (Fig. 6) show that the bore transformation that started with the initial trapezoidal-shaped bore at CG1 and developped over undular bores at CG2 to CG4 finally has provided trains of rank-ordered solitons. In this example, the plots show a total number of 16 solitons that are not completely separated yet in Fig. 6a at $x = 100\,\mathrm{m}$. Due to the different celerities of the solitons, they are nearly separated in Fig. 6c at $x = 230\,\mathrm{m}$ with the leading soliton being the largest and fastest. The simulated far-field data within this study provide the numerical amplitudes $A_{1,\mathrm{num}}$ of the leading solitons for further analyses.

TIME-DOMAIN ANALYSIS OF BORE DATA MEASUREMENTS

The time-domain analysis of the incident bores (e.g. as shown in Fig. 4 after zero-correction of the measured data) provides the initial bore height η_b. Due to variations and undulations within the initial bore plateaus over bore lengths in the measured data, the value for the bore height is determined within this study as the mean bore height $\overline{\eta_b}$ over the first 1/4 of the bore plateau.

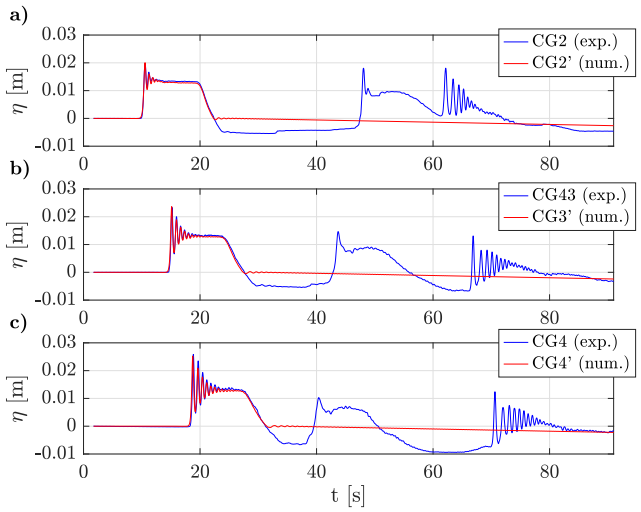

FIGURE 5: COMPARISON OF NEAR-FIELD DATA FOR TEST NO. 20 OBTAINED AT GAUGES CG2 TO CG4 (BLUE LINES) AND NUMERICAL SIMULATION DATA AT ACCORDING GAUGES CG2' TO CG4' (RED LINES).

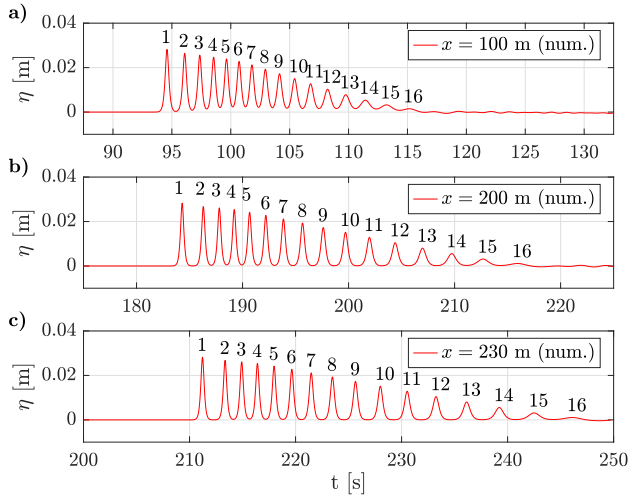

FIGURE 6: NUMERICAL FAR-FIELD SIMULATION DATA FOR TEST NO. 20 AT POSITIONS $x' = 100\,\mathrm{m}$, $200\,\mathrm{m}$ AND $230\,\mathrm{m}$.

The bore height can be given as η_b with respect to SWL or as total bore height h_b with respect to the the flume bottom (see Eq. (2)). The results for both expressions are presented in Fig. 7 as relative values with respect to the water depth, h_b/h_0 and η_b/h_0, as function of the bore Froude number, Fr_b, as calculated from the experimental data. The circles show the experimental values obtained from the time series measured in water depth $h = 0.1\,\mathrm{m}$ (blue data), and the triangles the data for $h = 0.2\,\mathrm{m}$ (black data). The lines present the values for h_b/h_0 (blue dashed line) and η_b/h_0 (black dot-dashed line) as function of the bore Froude number Fr_b in Eq. 4.

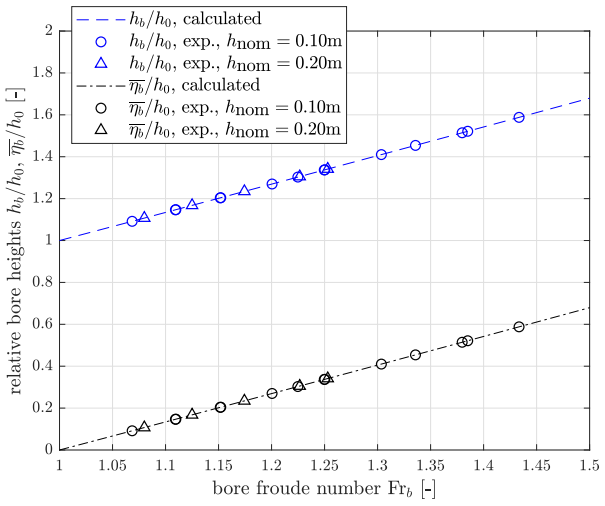

FIGURE 7: RELATIVE BORE HEIGHTS h_b/h_0 AND η_b/h_0 CALCULATED FROM EQ. (4) AND OBTAINED FROM MEASURED TIME SERIES.

KdV-NFT ON EXPERIMENTAL TEST DATA

Application of KdV-NFT to all tests provides nonlinear spectra analogous to the example in Fig. 2: All spectra are dominated by solitons, the radiation amplitudes are very small. Remember that in Fig. 2 the radiation amplitudes are superelevated by factor 100 in order to visualize them compared to the large soliton amplitudes. Thus, the radiation components are negligible for the bore propagation processes and, therefore, are not considered in the following analyses.

The soliton spectra (without the radiation components) for the first gauge CG1 of all analysed tests are presented in Fig. 8. The squares give the dimensional amplitudes for each soliton in the respective spectrum. Therefore, the amplitude of the largest and fastest soliton in each test is given by the leftmost square within one curve, the amplitude of the lowest and slowest soliton by the rightmost square. With reference to Eq. (8), Fig. 9 presents the soliton amplitudes as relative values with respect to the mean bore height $\overline{\eta_b}$ obtained from time-domain analysis. The expected relative value for the leading soliton according to Eq. (8), $A_1/\overline{\eta_b} = 2$, is given as dash-dotted line.

The results show that, independent of the actual dimensional amplitude, the relative amplitudes of all leading solitons are obtained as approximately twice the initial mean bore height, exactly as expected from Eq. (8). The reasons for the remaining deviations will be analysed in detail in future studies. Most probably,

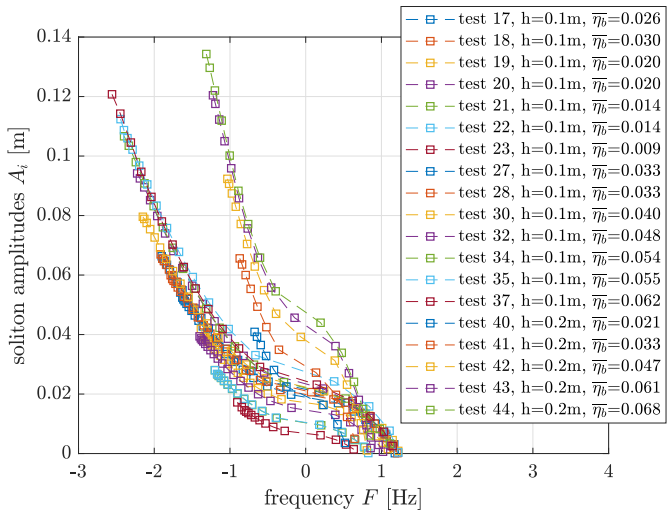

FIGURE 8: DIMENSIONAL SOLITON AMPLITUDES A_i AS OBTAINED FROM APPLICATION OF KdV-NFT ON EXPERIMENTAL TIME SERIES FROM GAUGE CG1.

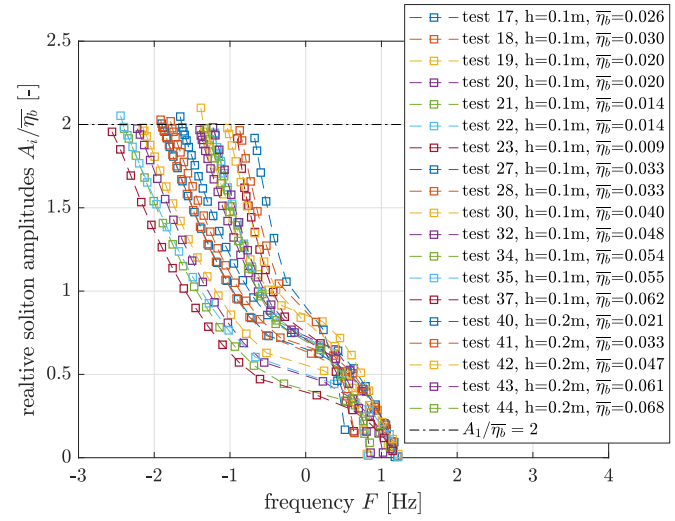

FIGURE 9: RELATIVE SOLITON AMPLITUDES $A_i/\overline{\eta_b}$ AS OBTAINED FROM APPLICATION OF KdV-NFT ON EXPERIMENTAL TIME SERIES FROM GAUGE CG1.

more sophisticated approaches of how to correctly determine the initial bore height from non-constant bore plateaus will improve the results.

ANALYSIS OF SOLITON PREDICTION FROM KdV-NFT

Figure 10 presents the comparison of the dimensional values of theoretical, experimental and numerical soliton amplitudes. The function for the calculated amplitude $A_1(h_b/h_0)$ according to

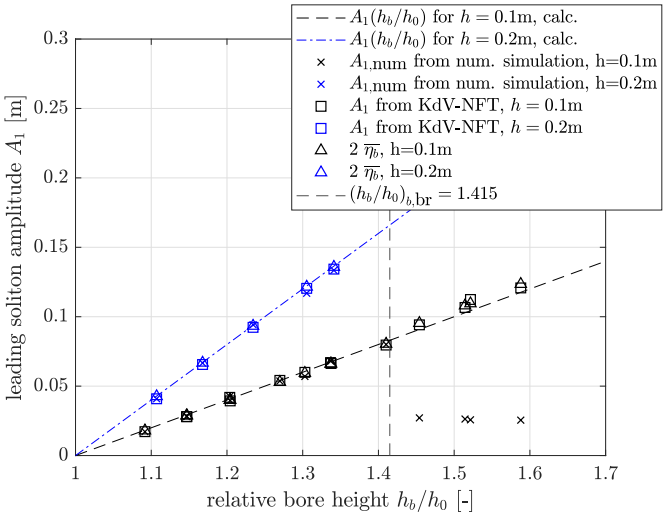

FIGURE 10: LEADING SOLITON AMPLITUDES FROM ANALYTICAL APPROACH, EMPIRICAL FORMULA, NUMERICAL SIMULATION AND SPECTRAL ANALYSIS USING KdV-NFT

Eq. (12) is given as dashed lines for both water depths, $h = 0.1$ m (black dashed line) and $h = 0.2$ m (blue dash-dotted line). The breaking limit of $(h_b/h_0)_{b,\mathrm{br}} = 1.415$ according to Lenau is plotted as grey-dashed line. The leading-soliton amplitudes $A_{1,\mathrm{num}}$ from the numerical simulations are given as black ($h = 0.1$ m) and blue ($h = 0.2$ m) crosses. The largest amplitudes as obtained from the nonlinear KdV-NFT spectra of the initial bore data from CG1 are plotted as black and blue squares for depths $h = 0.1$ m and $h = 0.2$ m, respectively. The empirical values based on Eq. (8) are given as triangles for depths $h = 0.1$ m (black) and $h = 0.2$ m (blue). The comparison of the leading-soliton amplitudes based on analytical approach, empirical formula, numerical simulation and nonlinear KdV-NFT spectra clearly shows, that the different methods provide the same results.

Finally, Fig. 11 shows the analysis results for both water-depths in non-dimensional representation. The black data show the relative amplitudes of the leading solitons A_1/h_0 with respect to the water depth, the blue data the amplitudes $A_1/\overline{\eta_b}$ over the mean bore height. The grey-dashed line divides the plot into non-breaking domain (with $h_b/h_0 \leq 1.415$) and the breaking domain ($h_b/h_0 > 1.415$). The black-dashed lines presents the calculated values $A_1(h_b/h_0)/h_0$ from Eq. (12). The results from KdV-NFT are plotted as squares in black for the non-breaking and in red for the breaking domain. The expected relative breaking height of the solitons based on the approach by Lenau [20] is given as black dot-dashed line at $H_b/h_0 = 0.83$. The results of the numerical simulations, $A_{1,\mathrm{num}}/h_0$, are plotted as black crosses. The relative values with respect to the mean bore height, $A_1/\overline{\eta_b}$, are plotted as blue and red triangles and blue crosses, respectively.

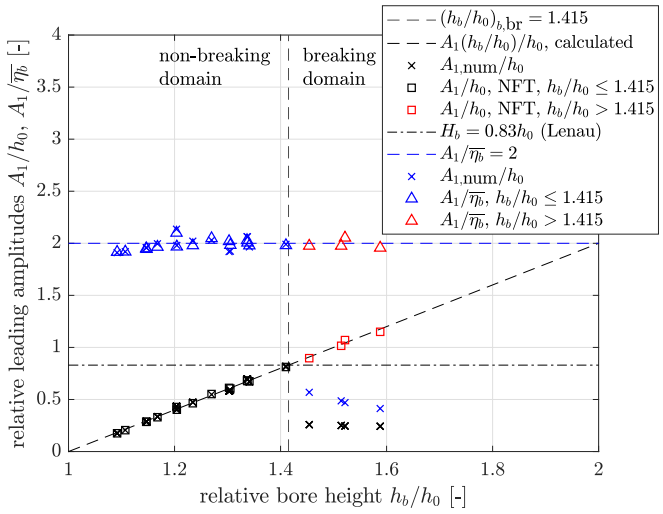

FIGURE 11: RELATIVE LEADING SOLITON AMPLITUDES A_1/h_0 AND $A_1/\overline{\eta_b}$.

The empirical value of $A_1/\overline{\eta_b} = 2$ is given as black-dashed line.

The grey-dashed line gives the relative bore height for the breaking limit, $(h_b/h_0)_{b,\mathrm{br}} = 1.415$. To the left of this value, the solitons are within the non-breaking domain. For the results obtained within this domain, the leading amplitudes from nonlinear spectral KdV-NFT analysis and numerical simulation agree very well and meet the expected values from analytical and empirical approaches.

To the right of the breaking limit, the obtained soliton amplitudes from analytical calculation and KdV-NFT are larger than the maximum amplitudes due to the breaking criterion. Unfortunately, wave breaking is neither included in the analytical equation nor in the KdV equation. Therefore, the breaking limit of the solitons is not considered within these approaches. Empirical observations show that, starting at a certain Froude number and depending on the actual height of the soliton, the solitons that evolve out of the bore front start to break. Therefore, soliton amplitudes derived from the nonlinear KdV-NFT spectra that are larger than the breaking criterion, i.e. from bores with initial values $h_b/h_0 > 1.415$, are plotted in red. The numerical results for relative bore heights above the breaking limit clearly show that the amplitudes of the leading solitons are significantly affected by the wave breaking process. The observed data as plotted around $A_1 \approx 0.025\,\mathrm{m}$ give the amplitude of the discrete solitons in the far-field that emerged from the breaking bore. Nevertheless, the data clearly show that the analytical, the empirical, and the spectral approach do not consider the effects of wave breaking. Thus, these data need further research in order to research the amplitude behaviour here and to combine the KdV-NFT analysis results with the physical limitations due to wave breaking.

SUMMARY AND OUTLOOK

Within this study, the KdV-based nonlinear Fourier transform was applied to experimental test data with non-breaking and breaking undular bore propagation in constant depth. The experimental results were furthermore verified using numerical simulations for the far-field propagation of the bores in COULWAVE. For comparison, the expected values for bore height and amplitude of the leading solitons have been calculated based on water depth, mean bore height, and relative bore height. The predicted soliton amplitudes obtained from the KdV-NFT analysis of the initial bore bore meet the results from analytical calculation, empirical formula and numerical simulations as long as the bores stay below the breaking limit, $h_b/h_0 \leq 1.415$.

These results confirm that the application of KdV-NFT on the initial trapezoidal-shaped near-field data measured at the first gauge already characterises the far-field behaviour of the bore completely. While propagating in constant depth and without wave breaking, the initial nonlinear amplitude spectrum as considered in this paper is invariant while the so-called phase spectrum is changing. Therefore, all spectral information for the bore propagation and the far-field train of solitons is already completely known from this near-field gauge position. Thus, the results clearly show that the near-field KdV-NFT spectrum allows the reliable prediction of the far field data, including the amplitude of the leading soliton.

We point out that even if the leading-soliton amplitude can be simply determined by the analytical or empirical approach, the application of KdV-NFT has a huge advantage over the conventional methods: The KdV-NFT spectrum provides *all* solitons within the data with correct amplitudes, not just the leading one. Without KdV-NFT, extensive numerical simulations are required to simulate the complete disintegration of the initial bore in order to obtain the same results. For the bore analysed within this study, relative simulation lengths of more than 1500 times the initial depth have been necessary to get all solitons separated from each other. Therefore, application of KdV-NFT provides these results much faster.

Future analyses will provide a more detailed analysis of the number and amplitudes of all solitons determined within the initial bore. Knowledge on the spectral basic components will help to obtain further insight into the nonlinear processes governing the propagation of bores and tsunamis. Furthermore, the effect of wave breaking on the analysis results will be investigated in order to avoid false results from the spectral analysis.

ACKNOWLEDGEMENTS

This project has received funding from the European Research Council (ERC) under the European Union's Horizon 2020 research and innovation programme (grant agreement No 716669).

REFERENCES

[1] El, G.A. *Korteweg–de Vries equation: solitons and undular bores*. In book: Solitary Waves in Fluids, Advances in Fluid Mechanics, Ed.: Grimshaw, R.H.J., WIT Press.

[2] Gavrilyuk, S.L., Liapidevskii, V.Y. and Chesnokov, A. A., 2016. "Spilling breakers in shallow water: applications to Favre waves and to the shoaling and breaking of solitary waves". *Journal of Fluid Mechanics,* ***808***, pp. 441–468.

[3] Peregrine, D.H., 2006. "Calculations of the development of an undular bore". *Journal of Fluid Mechanics,* ***25***(2), pp. 321–330.

[4] Brühl, M., 2014. "Direct and inverse nonlinear Fourier transform based on the Korteweg–de Vries equation (KdV-NLFT) - A spectral analysis of nonlinear surface waves in shallow water. Dissertation. (http://www.digibib.tu-bs.de/?docid=00058144)". Ph.D. thesis, TU Braunschweig.

[5] Brühl, M. and Oumeraci, H., 2012. "Nonlinear decomposition of transmitted wave trains from soliton fission using "Nonlinear Fourier transform (NLFT)": The spectral basic components (OMAE2012-83418)".

[6] Brühl, M. and Oumeraci, H., 2016. "Analysis of long-period cosine-wave dispersion in very shallow water using nonlinear Fourier transform based on KdV equation". *Applied Ocean Research,* ***61***, pp. 81–91.

[7] Osborne, A.R., 2010. *Nonlinear ocean waves and the inverse scattering transform*. Elsevier, Amsterdam.

[8] Brühl, M., Ujvary, S., Barranco Granged, I., Prins, P.J., Wahls, S. and Liu, P.L.-F., 2020. "Analysis of bore propagation using the KdV-based nonlinear Fourier transform (KdV-NFT)". *(in preparation)*.

[9] Stoker, J.J., 1957. *Water waves: The mathematical theory with applications*. Wiley, New York.

[10] Miller, R.L., 1968. "Experimental determination of run-up of undular and fully developed bores". *J. Geophys. Res.,* ***73***(14), pp. 4497–4510.

[11] Yeh, H.H., Ghazali, A. and Marton, I., 1989. "Experimental study of bore run-up". *J. Fluid Mech.,* ***206***, pp. 563–578.

[12] Ligett, James A., 1994. *Fluid Mechanics*, New Ed. ed. McGraw.

[13] Favre, H., 1935. *Ondes de translation*. Duno, Paris.

[14] Treske, A., 1994. "Undular bores (Favre waves) - experimental studies". *J. Hydr. Res.,* ***32***, pp. 355–370.

[15] Stansby, P.K., Chegini, A. and Barnes, T.C.D., 1998. "The initial stages of dam-break flow". *J. Fluid Mech.,* ***374***, pp. 407–424.

[16] Ismail, H., Abd Wahab, A.K. and Alias, N.E., 2012. "Determination of mangrove forest performance in reducing tsunami run-up using physical models". *Natural Hazards,* ***63***(2), pp. 939–963.

[17] Barranco Granged, I., 2020. "Surf and swash flows generated by transient long waves". Ph.D. thesis (in preparation), NUS Singapore.

[18] Robert G. Dean and Robert A. Dalrymple, 1991. *Water Wave Mechanics for Engineers and Scientists*. World Scientific, Singapore.

[19] Brühl, M., Büchner, E. and Zhang, H., 2018. "Amplitudes of landslide-generated impulse waves from nonlinear Fourier transform as function of the slide characteristics". Proc. 7th International Conference on the Application of Physical Modelling in Coastal and Port Engineering and Science (Coastlab18).

[20] Lenau, W.C., 1966. "The solitary wave maximum amplitude". *Journal of Fluid Mechanics,* ***26(02)***, p. 309.

[21] McCowan, J., 1894. "On the highest wave of permanent type". *Philos. Mag.,* ***5***(38), pp. 351–359.

[22] Korteweg, D.J. and de Vries, G., 1895. "On the change of form of long waves advancing in a rectangular canal, and on a new type of long stationary waves". *Philos. Mag. Ser.,* ***5***(39), pp. 422–443.

[23] Whitham, G.B., 1974. *Linear and Nonlinear Waves*. Wiley, New York.

[24] Miles, J.W., 1980. "Solitary waves". *Annu. Rev. Fluid Mech.,* ***12***, pp. 11–43.

[25] Osborne, A.R., 1993. "The behaviour of Solitons in Random-Function Solutions of the Periodic Korteweg–de Vries Equation". *Physical Review Letters,* ***71***(19), pp. 3115–3118.

[26] Antonova, M. and Biswas, A., 2009. "Adiabatic parameter dynamics of perturbed solitary waves". *Communications in Nonlinear Science and Numerical Simulation,* ***14***(3), pp. 734–748.

[27] Girgis, L. and Biswas, A., 2010. "Soliton perturbation theory for nonlinear wave equations". *Applied Mathematics and Computation,* ***216***(7), pp. 2226–2231.

[28] Dubrovin, B.A. and Novikov, S.P., 1975. "Periodic and conditionally periodic analogs of the many-soliton solution of the KdV-equation". *Soviet Physics JETP,* ***40***, p. 1058.

[29] Osborne, A.R., 1995. "Soliton physics and the periodic inverse scattering transform". *Physica D,* ***86***, pp. 81–89.

[30] Brühl, M. and Oumeraci, H., 2014. "Nonlinear Fourier transform (NLFT) for the identification of transmitted solitons behind submerged reefs: The reconstruction of the original data (OMAE2014-24162)".

[31] Zhang, H. and Brühl, M. "Generation of transient extreme waves by inverse KdV-NLFT based nonlinear Fourier transform (KdV-NLFT)". Proc. 9th Chinese-German Joint Symposium on Hydraulic and Ocean Engineering (CGJoint2018).

[32] Lynett, P.J., Liu, P.L.-F., Sitanggang, K.I. and Kim, D.-H. Modeling wave generation, evolution and interaction with depth-integrated, dispersive wave equations. COULWAVE code manual. Cornell university long and intermediate wave modeling package v. 2.0.